First-Principles Study of Water Confined in Single-Walled Silicon Carbide Nanotubes

ARTICLE *in* THE JOURNAL OF PHYSICAL CHEMISTRY C · AUGUST 2011

Impact Factor: 4.77 · DOI: 10.1021/jp201882d

THE JOURNAL OF PHYSICAL CHEMISTRY C

ARTICLE

pubs.acs.org/JPCC

First-Principles Study of Water Confined in Single-Walled Silicon Carbide Nanotubes

Rui Yang,*[,†,§] Tamsyn A. Hilder,[‡] Shin-Ho Chung,[‡] and Alistair Rendell[†]

[†]School of Computer Science and [‡]Research School of Biology, Australian National University, Canberra, ACT 0200 Australia

ABSTRACT: In the present work, water molecules confined inside single-walled silicon carbide nanotubes (SiCNTs) are studied using density functional theory calculations. A set of periodic boundary condition models are established for segments of single-file water chains, infinite single-file water chains, and infinite multifiled water networks encapsulated within the periodic armchair and zigzag SiCNTs with (5,5), (6,6), (8,0), (9,0), and (10,0) chiralities. Two hybrid density functionals with and without dispersion correction, ωB97XD and B3LYP, respectively, are employed in all calculations for structure, interaction energy, and charge analysis. Although the silicon carbide surface is essentially hydrophilic, water molecules within SiCNTs have structures and properties that resemble those in the hydrophobic single-walled carbon nanotube since both are controlled by the geometry confinement. It is necessary to include dispersion corrections to describe the weak interactions between the water molecules and the SiCNT wall which arise mainly from van der Waals interactions and a slight charge transfer from SiCNT to the enclosed water molecules.

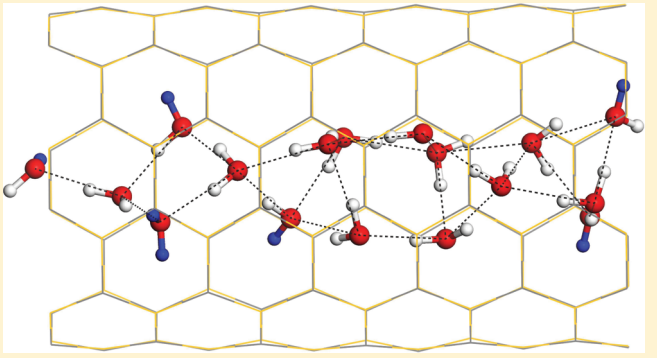

INTRODUCTION

In recent decades, nanoscale water in confined environments has attracted considerable attention owing to its great importance in many systems of science, including biology, molecular devices, nanofluidic devices, inorganic materials, electronic devices, and geology. It has enormous promise in substantially improving the performance and efficiency of many applications such as biological/chemical systems,[1−3] water purification systems,[4] and fuel cell devices.[5] In addition, the spatial dimensions of nanotubes are comparable to those of biological ion channels providing a simple model environment to understand the primary behavior of water in complex biological systems.

With the development of new experimental and computational facilities and technologies, the behavior of water molecules at the nanoscale has been extensively investigated. For example, water molecules have been filled into carbon nanotubes (CNTs) experimentally, and the in situ high-resolution study of water confined in a multiwalled CNT system has been reported.[6,7] Neutron scattering experiments also show entry of water into an open-ended single-walled nanotube and identified an ice-like water structure.[8]

It is expected that water molecules confined in nanometer-sized channels or pores have structural, transport, and thermodynamics properties different from those of bulk liquid water due to the influences of the water−wall interactions, the small channel diameter, and hydrogen bonding between the water molecules.[9−16] Koga et al. found that, when confined inside a single-walled carbon nanotube (SWCNT) under axial pressure, water can exhibit a first-order freezing transition to hexagonal and heptagonal ice nanotubes and a continuous phase transformation into solid-like square or pentagonal nanotubes.[15] In 2006, Holt and co-workers experimentally found that the water flow rate through a CNT with a radius of 1−2 nm was more than 3 orders of magnitude faster than the conventional nonslip hydrodynamic flow.[12] Hummer et al. also reported fast water transport in CNTs using classical molecular dynamics (MD) simulations.[9] For smaller diameter tubes (8.1 Å), they found that water diffusion occurs as a burst-like mechanism, stemming from the presence of single-file water chains capable of moving with little resistance.

When water is confined in very narrow nanochannels with appropriate radii, the water molecules form a hydrogen-bonded single-file chain.[9] The unique dynamic property of confined water within CNT arises from the weak interaction between the water molecules and the hydrophobic CNT and the hydrogen bonding in the single-file water chain.

Since CNTs possess extraordinary physical and chemical properties, the behavior of the water molecules encapsulated inside the CNT system has been extensively investigated.[17] Recently, the study on the nanoscale water in confined environments has been extended to nanotube systems of other elements, such as a boron nitride nanotube (BNNT). Won and Aluru reported that the (5, 5) BNNT can conduct water owing to the comparatively strong interactions between N atoms on the

Received: February 26, 2011
Revised: July 25, 2011
Published: July 26, 2011

BNNT and water molecules, which makes BNNT a promising alternative ion-channel candidate to CNT.[18] A further study by Won and Aluru based on first-principles density functional theory (DFT) and molecular dynamics (MD) simulations revealed that the wetting behavior of a (5,5) BNNT is improved by the presence of partial charges.[19] The water diffusion and structure are also affected by the diameter of the particular BNNT. Yuan and Zhao revealed that the charge redistribution in a water-filled single-walled BNNT can generate a voltage of several millivolts between the two ends of the tube, which make the system a promising candidate for a synthetic nanoscale power cell and as a practical nanopower harvesting device.[20]

More recently, SiCNT has been successfully synthesized by several different groups.[21−29] Similar to the BNNT, it has a large band gap, possesses a reactive exterior surface that facilitates sidewall decoration, and has stability at high temperature.[30,31] As a result, both BNNT and SiCNT have potential applications as a replacement for CNTs in electronic devices operating under harsh conditions of high temperature, power, and frequency.[32]

Given that SiCNTs may possess unique properties, it is of interest to study the potential application of SiCNT to biological science such as for molecular channels to transport water or ions. Unlike the CNT and BNNT systems, there have been no studies on the structures and properties of water confined inside SiCNT systems. In contrast to the CNT's hydrophobic surface, the SiC surface is hydrophilic.[33] It is reported that hydrophilic and hydrophobic nanotubes may have different abilities to transport water.[34]

In this paper, we examine the structures and properties of water molecules confined in a variety of SiCNT systems. We first present the computational methods and models in Section II, and then the structures, energies, and electronic property are analyzed in Section III. Finally, in Section IV, we list some of the salient points uncovered from our computational studies.

MODELS AND COMPUTATIONAL METHODS

We focus on two chiralities of SiCNT systems, namely, armchair and zigzag. For both chiralities, only type-1 arrangements were considered. These systems have alternating Si and C atoms with each Si atom having three C neighbors and vice versa and are energetically preferred over alternative arrangements containing C−C and Si−Si bonds.[35,36] Also, only structures with diameters large enough to contain water molecules were used, i.e., (5, 5), (6, 6), (8, 0), (9, 0), and (10, 0). All SiCNT models are built with a single supercell containing six hexagonal rings along the length of the nanotube. With the exception of (6, 6) SiCNT, six or seven water molecules were placed in each SiCNT with random orientations. For SiCNT(6,6), with a much larger diameter (over 10 Å), 17 water molecules were placed in it. This number was chosen to give a number density comparable to that of bulk water.

The structures of the various systems were initially optimized by performing plane wave basis pseudopotential calculations using the CPMD package.[37] The supercells in the three-dimensional periodic boundary condition (PBC) model were 15 Å in the x- and y-axis to leave enough vacuum space between the real and image nanotubes, with the infinite nanotubes lying along the z-axis. The geometry optimizations were performed using the Limited-memory Broyden−Fletcher−Goldfarb−Shanno (LBFGS) algorithm with a variable-cell vector. All calculations were conducted using the BLYP-type GGA functional with norm-conserving Troullier−Martins pseudopotentials in the Kleinman−Bylander separable form. The wave functions were expanded using a plane-wave basis set with a kinetic energy cutoff of 80 Ry.

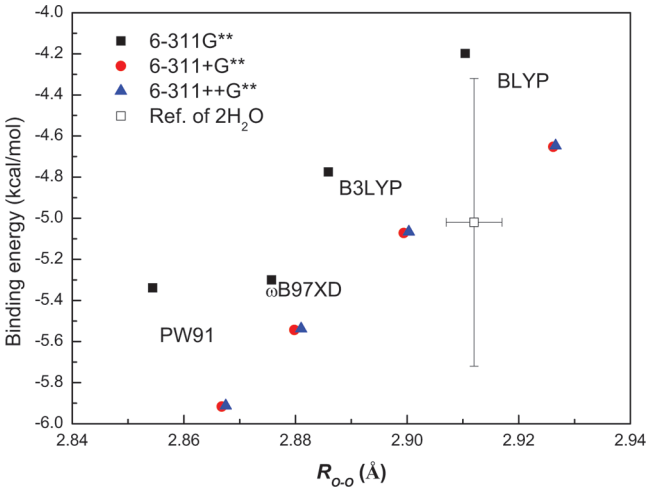

Figure 1. Optimized structure and binding energy of the global minimum structure of water dimer.

On the basis of the optimized structures obtained from the above first-principles plane wave pseudopotential calculations, further geometry optimizations were conducted using DFT calculations as implemented in the Gaussian 09 package.[38] This code uses a localized Gaussian basis that allows the study of one-dimensional infinite nanotube structures without interactions with imaging nanotubes. All optimization processes are performed until the maximum/root-mean-square force on a single atom converged to less than 0.00045/0.0003 au and maximum/root-mean-square displacement converged to less than 0.0018/0.0012 au.

It is well-known that both local density approximation (LDA) and generalized gradient approximation (GGA) DFT cannot accurately reproduce dispersive or van der Waals interactions. These interactions are potentially significant for water in a confined space. In an attempt to account for this, we performed a series of benchmark calculations on the structure and binding energy of water dimer using different DFT functionals. The purpose of these calculations was to verify the accuracy of our simulation setup and to provide information on the ability of different functionals to account for the sort of intermolecular interactions that are of importance. The benchmark calculations include use of the BLYP GGA functional and the B3LYP hybrid method. The PW91 GGA functional was also considered as it has been reported to be able to represent hydrogen bonding well.[39] In addition, we also used the ωB97XD dispersion corrected hydrid DFT method.[40] Various sizes of split valence basis sets with polarized and diffuse functions were employed, including the 6-311 g**, 6-311+g**, and 6-311++g** sets as implemented in Gaussian 09. Binding energy computations were performed using the counterpoise method to correct for basis set superposition errors (BSSE).

The distances between the two oxygen atoms, R_{O-O}, and the binding energies between the two water molecules in a water dimer calculated using the various basis sets and DFT methods are shown in Figure 1. These values are compared with the reported values of 2.912 Å for the bond length

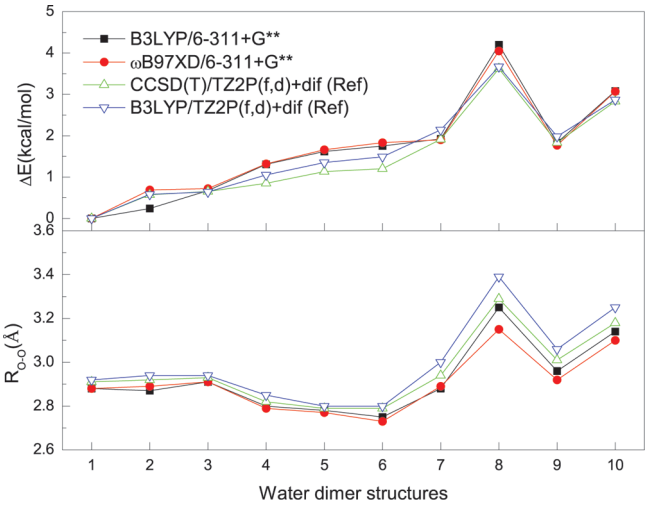

Figure 2. Relative binding energy ΔE and R_{O-O} of different water dimer stationary structures: 1, nonplanar open C_s (global minimum); 2, open C_1; 3, planar open C_s; 4, cyclic C_i; 5, cyclic C_2; 6, doubly bifurcated C_{2h}; 7, triply hydrogen bonded C_s; 8, doubly bifurcated C_2h; 9, nonplanar bifurcated C_{2v}; 10, planar bifurcated C_2v. The two sets of reference values of CCSD(T)/TZ2P(f,d)+dif and B3LYP/TZ2P(f,d) +dif from refs 42 and 43, respectively.

and −5.02 kcal/mol for the binding energy given by Klopper et al. in their extensive computational study of water dimer.[41] Error bars have been added to indicate values that are within a range of 0.005 Å for the bond length and 0.7 kcal/mol for the energy of the results of Klopper et al.

It is noted that the two GGA functionals, BLYP and PW91, tend to overestimate or underestimate the R_{O-O} distance and the binding energy. The hybrid function B3LYP in conjunction with the 6-311+g** or 6-311++g** basis sets can reproduce the R_{O-O} distance and the binding energy of Klopper et al.[41] with the smallest error. The ωB97XD results have shorter R_{O-O} distances and stronger binding energies than the B3LYP results owing to the additional attractive contribution of the dispersion correction.

The calculated hydrogen bond angle is 175.0° and 175.2° for the B3LYP/6-311++g** and ωB97XD/6-311++g** calculations, respectively; these lie within 0.5% of the reference value of 174.5°.[41]

The performance of the two hybrid DFT functionals was examined further by considering the ten other stationary points on the water dimer potential energy surface identified by Anderson and Tschumper.[42,43] Starting from each of these structures, geometry optimizations were performed using the B3LYP/6-311+g** and ωB97XD/6-311+g** methods. For these structures, the distances between the two oxygen atoms, R_{O-O}, and the energies of the optimized water dimer stationary structures relative to the energy of the global minimum, ΔE, are shown in Figure 2. For comparison, the reported values obtained using the CCSD(T) and B3LYP methods in combination with a TZ2P(f,d)+diffusion basis are also shown.

From the above, it is clear that both the B3LYP/6-311+g** and ωB97XD/6-311+g** methods can reproduce well the reported energetic and structural ordering obtained using the B3LYP and CCSD(T) methods and the large triple-ζ basis set.[42,43] The largest difference is for the distance between the oxygen atoms, which is a bit shorter in the ωB97XD calculations due to the additional dispersive contribution.

Table 1. Calculated C−Si Bond Length, d_{C-Si}, and Diameters of SiCNTs Compared with Reference Values (in Å)

	d_{C-Si}		diameter		
chirality	B3LYP	ωB97XD	B3LYP	ωB97XD	reference
(4,4)	1.794	1.785	6.890	6.853	7.022[36]
(5,5)	1.792	1.784	8.590	8.547	8.620[44,30]
					8.640[32]
					8.760[36]
(6,6)	1.792	1.783	10.293	10.244	10.2[45]
					10.3[46]
					10.451[36]
(7,7)	1.791	1.783	11.997	11.941	12.03[47]
					12.05[30]
(8,0)	1.793	1.785	7.983	7.946	7.87[47]
					7.90[45]
					8.00[46]
					8.01[32]
					8.06[44]
					8.074[35]
(9,0)	1.792	1.784	8.958	8.916	8.89[47]
					9.05[35]
(10,0)	1.792	1.784	9.936	9.890	9.95[30]
					10.047[35]

On the basis of the above analysis, the B3LYP methods were employed in this work, and ωB97XD was used to evaluate the effect of dispersion. As both the 6-311+g** and 6-311++g** basis sets gave similar results, the former computationally cheaper basis set was employed for the water molecules. This was combined with a smaller 6-31g* basis on the Si and C atoms in SiCNT. The validity of the SiCNT basis set is considered in the next section.

To identify the interaction between the water and the SiCNT, we define the coupling energy per water molecule using the following formula

$$E_C = (E_{complex} - E_{SiCNT} - E_{nH_2O})/n \quad (1)$$

where $E_{complex}$ is the total energy of the SiCNT complex with the nH_2O confined within it and E_{SiCNT} and E_{nH2O} are the energies of the isolated SiCNT and nH_2O systems using the same geometries as in the complex.

To characterize the interwater interaction, we define the binding energy per water molecule as follows

$$E_B = (E_{complex} - E_{SiCNT} - \sum_{i=1,n} E^i_{H_2O})/n \quad (2)$$

where $E_{complex}$ and E_{SiCNT} have the same meaning as in eq 1, while $\sum_{i=1,n} E^i_{H2O}$ sums the total energy of each individual water molecule. E_B measures the average interaction between a water molecule and its environment, including the contributions to E_C and the hydrogen bonding from a water molecule. As a result, the hydrogen bonding strength per water molecule, E_{H-bond} can be evaluated as the difference between E_B and E_C, i.e.

$$E_{H-bond} = E_B - E_C \quad (3)$$

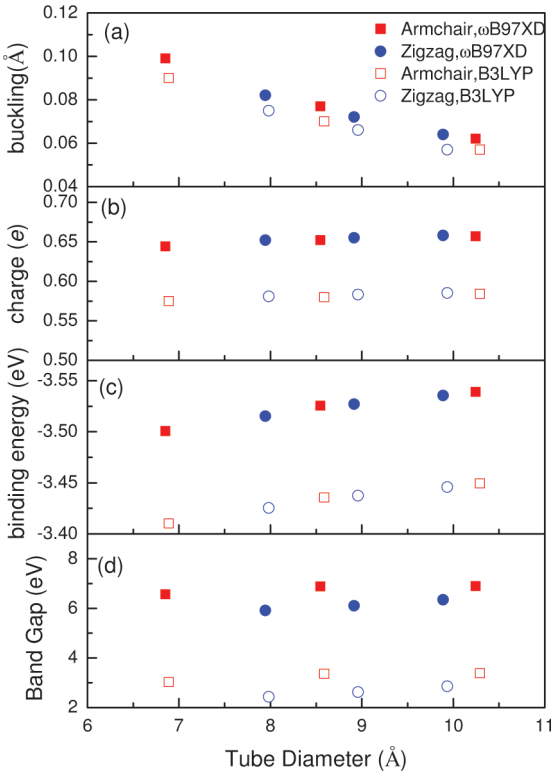

Figure 3. Diameter dependence of (a) buckling structure, (b) atomic charge, (c) binding energy, and the (d) band gap in several armchair and zigzag SiCNTs spanning (4, 4), (5, 5), (6, 6), (8, 0), (9, 0), and (10, 0) by using B3LYP and ωB97XD functionals.

RESULTS AND DISCUSSION

SiCNT Systems. We first consider the equilibrium configurations for the (4,4), (5,5), (6,6), (7,7), (8,0), (9,0), and (10,0) series of SiCNTs and compare them with those reported results.[30,32,35,36,44−47]

The C−Si bond length, d_{C-Si}, and diameter of each SiCNT are listed in Table 1. For all SiCNTs, the d_{C-Si} values calculated using B3LYP are approximately 1.79 Å and are in good agreement with the reference value of 1.80 Å obtained from other ab initio results.[32] The value of d_{C-Si} becomes slightly shorter with increasing index for both armchair and zigzag chiralities. The ωB97XD-type hybrid DFT gives a d_{C-Si} distance of approximately 1.785 Å that is shorter compared to B3LYP. The diameter of SiCNT is defined as the average diameter of the Si and C rings. As a result of the slightly larger d_{C-Si}, the average diameter is slightly larger when using B3LYP compared to ωB97XD. All diameters match well with those reported by a variety of other theoretical studies as shown in Table 1.

For all optimized SiCNTs, the less electronegative Si atoms locate closer to the tube axis than the C atoms. Such reconstruction is reminiscent of that seen for group-III nitride nanotubes where the more electronegative N atoms are located outward relative to the group-III atoms.[48] In this paper, the radial buckling is calculated by subtracting the mean Si radius from the mean C radius.

As shown in Figure 3(a), the buckling effect becomes weaker with increasing tube diameter regardless of chirality. This agrees well with other reported theoretical studies on SiCNT.[32,36] The amount of buckling is comparable between the two hybrid DFT functionals. The same trend was found for BNNT, which has a similar arrangement of alternating (B and N) atoms.[49]

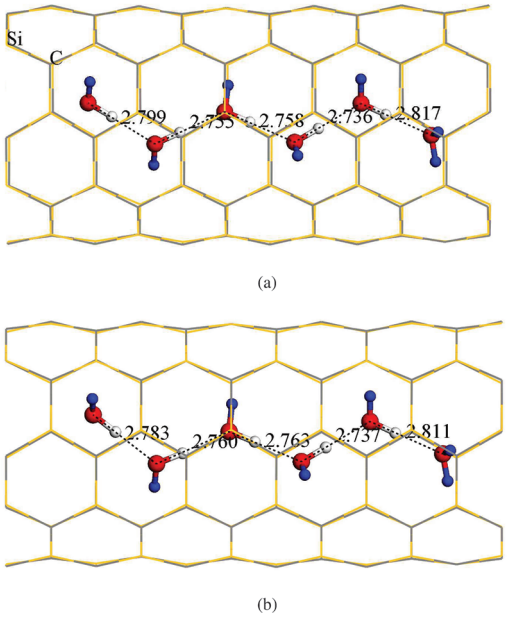

Figure 4. $(H_2O)_6$ chain confined within SiCNT(5,5) by using (a) B3LYP and (b) ωB97XD functionals. The red, white, and blue spheres represent oxygen, hydrogen-bonded, and non-hydrogen-bonded hydrogen atoms, respectively.

We have also performed Mulliken charge analysis for the SiCNT systems as shown in Figure 3(b). All structures show significant electron transfer from Si to C atoms owing to the greater electronegativity of C atoms compared to Si atoms. The amount of charge transfer increases slightly with increasing tube diameter, which is consistent with other studies.[36] The calculated charge on the Si atoms lies around 0.55e and 0.65e when evaluated using the B3LYP and ωB97XD functional, respectively. These values agree well with another reported ab initio result of 0.60e.[50]

With increasing tube diameter, the binding energy of SiCNT increases slightly as shown in Figure 3(c). Again, this trend agrees with other ab initio calculations.[32,35,36] Also, as for BN, AlN, and GaN nanotube systems, the binding energies for SiCNT systems are relatively insensitive to the chirality of the tube.[51−53]

The calculated band gap of both the armchair and zigzag SiCNTs gets larger with increasing nanotube diameter as shown in Figure 3(d). This is due to a lowering of the HOMO energy that results from antiphase interactions in the SiCNT.[54] A similar dependence of the band gap on tube diameter has also been reported in other first-principles computations.[32] As expected, the studied zigzag SiCNTs have a direct band gap, whereas the armchair ones have an indirect band gap.

In summary, the DFT functionals and basis sets employed in the present work appear to be able to give reliable structures, energies, and electronic properties for all the studied SiCNTs. We now consider water molecules confined within the SiCNTs.

Water-Confined SiCNT Systems. For the various SiCNT systems considered here, three types of water configurations were observed: (i) single-file water chain fragments which occurred for the SiCNT(5,5) system with six and seven water

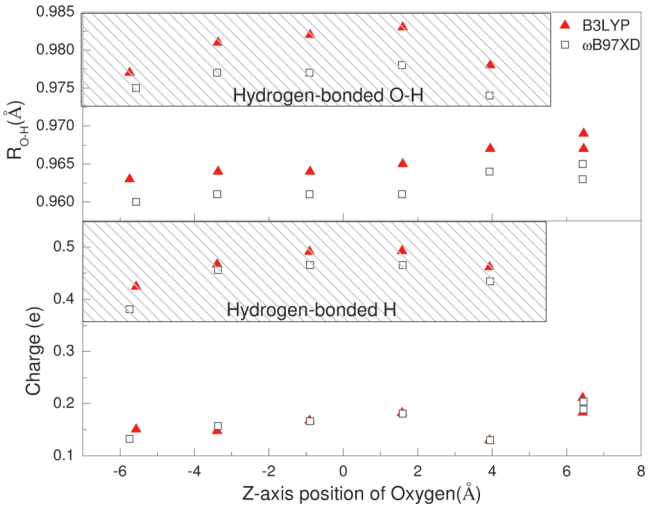

Figure 5. R_{O-H} and charge of H atoms of the $(H_2O)_6$ chain within SiCNT(5,5).

molecules, (ii) infinite single-file water chains which occurred for the SiCNT(8,0), (9,0), and (10,0) systems with six and seven water molecules, and (iii) infinite multifiled water networks which occurred for the 17 water molecule SiCNT(6,6) system. These will now be considered in turn.

Water Chain Fragments in SiCNT(5,5). Starting from random positions, six water molecules confined within SiCNT(5,5) tend to form an ordered water chain fragment as shown in Figure 4 for both B3LYP and ωB97XD functionals.

Each water molecule is hydrogen-bonded to one or two neighboring water molecules to form a zigzag chain with a roughly equal R_{O-O} distance between neighboring oxygen atoms. Similar chainlike encapsulated waters have been observed in many other systems using a variety of simulation techniques.[55] Using geometric criteria, a pair of water molecules can be interpreted as being hydrogen bonded if the R_{O-O} distance is less than 3.6 Å, the R_{O-H} distance between the acceptor oxygen and the donor hydrogen atom is less than 2.4 Å, and the hydrogen bonded O−H···O angle is less than 30°.[56,57] Using these criteria, there are five hydrogen bonds in the $(H_2O)_6$ chain. These aligned the chain with the nanotube axis, with alternate hydrogen bonds flipping direction about the axis as shown by the dotted lines in Figure 4. The average R_{O-O} in the $(H_2O)_6$ chain is 2.773 Å in the B3LYP calculations, which is less than that in a gas-phase water dimer (2.91 Å) when using the same level of theory. The water alignments for the ωB97XD functional (also shown in Figure 4) are similar to those for the B3LYP functional, as is the average value of R_{O-O} at 2.771 Å.

There are seven non-hydrogen-bonded O−H covalent bonds in the $(H_2O)_6$ chain pointing to the SiCNT wall (perpendicular to the tube axis). These are indicated by the small blue spheres in Figure 4. This includes the two hydrogen atoms on the right most water molecule of the $(H_2O)_6$ chain where the two dangling O−H bonds point vertically. This is regarded as the energetically preferred orientation for a single water molecule in a carbon nanotube.[55]

We also calculate the Mulliken charge on each H atom and plot this together with the R_{O-H} distance as a function of position along the *z*-axis of the nanotube in Figure 5.

This figure shows that the hydrogen atoms can be classified into two distinct groups. The hydrogen-bonded H atoms have

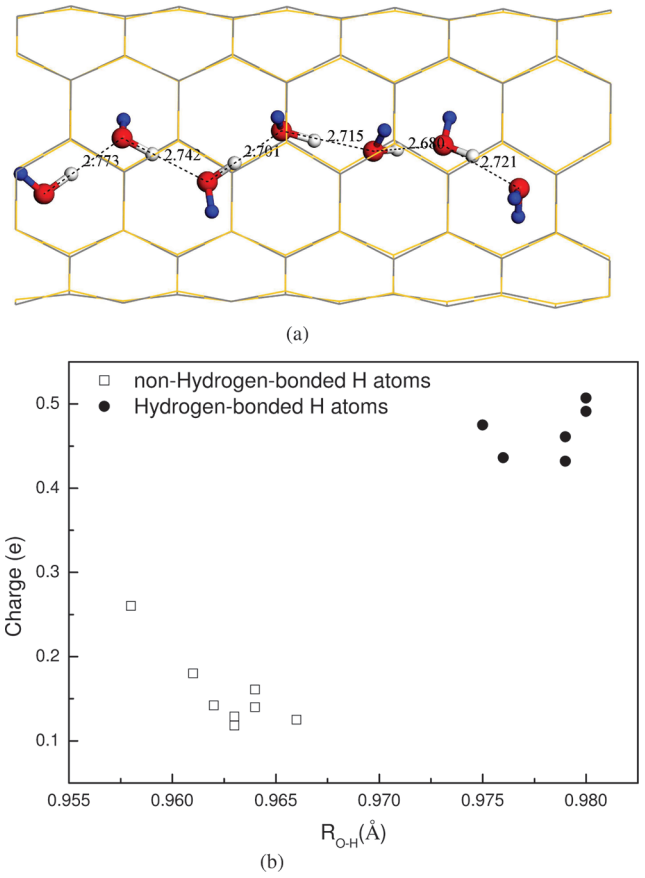

Figure 6. Structure and R-C plot of the $(H_2O)_7$ chain within SiCNT(5,5).

larger R_{O-H} values of around 0.972−0.985 Å compared to the non-hydrogen-bonded values of around 0.960−0.970 Å. The average R_{O-H} values for the non-hydrogen-bonded and hydrogen-bonded O−H bonds are 0.968 and 0.983 Å, respectively; this is comparable to the R_{O-H} values of 0.973 and 1.005 Å that were obtained for an infinitely long water chain confined within SWCNT(6,6) using first-principles molecular dynamics methods.[58] The hydrogen-bonded hydrogen atoms also have larger charges (average at 0.467e) than the non-hydrogen-bonded ones (average at 0.167e), indicating that the hydrogen atoms become more ionic when hydrogen bonded. For the water molecule on the far right of the chain, both the R_{O-H} values and the Mulliken charges indicate that neither H atom in this molecule is hydrogen-bonded. This confirms that the $(H_2O)_6$ structure is a chain fragment. Finally, it is noted that there are only slight differences in R_{O-H} and charge values between the B3LYP and ωB97XD functionals. Recalling that both DFT functionals also give rise to very similar geometries for the $(H_2O)_6$ chain (as shown in Figure 4), it can be concluded that the equilibrium configuration and electronic structure of the confined water chains are relatively insensitive to the selected DFT functional. Thus, only structural and charge results obtained using the ωB97XD functional will be presented below.

Similar to the previous system, seven water molecules encapsulated inside the SiCNT(5,5) also align into a 1D water chain as shown in Figure 6(a). The average R_{O-O} of the $(H_2O)_7$ chain is 2.722 Å, which is less than that of the six-water chain at 2.771 Å. This trend of decreasing R_{O-O} distance with increasing

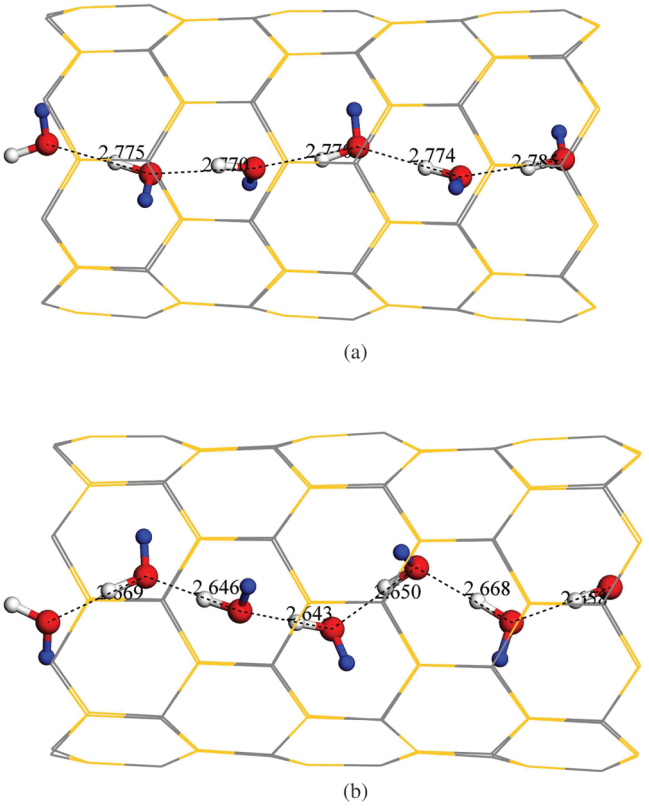

Figure 7. Water chain structure confined in SiCNT(8,0). (a) Six-water chain in SiCNT(8,0). (b) Seven-water chain in SiCNT(8,0).

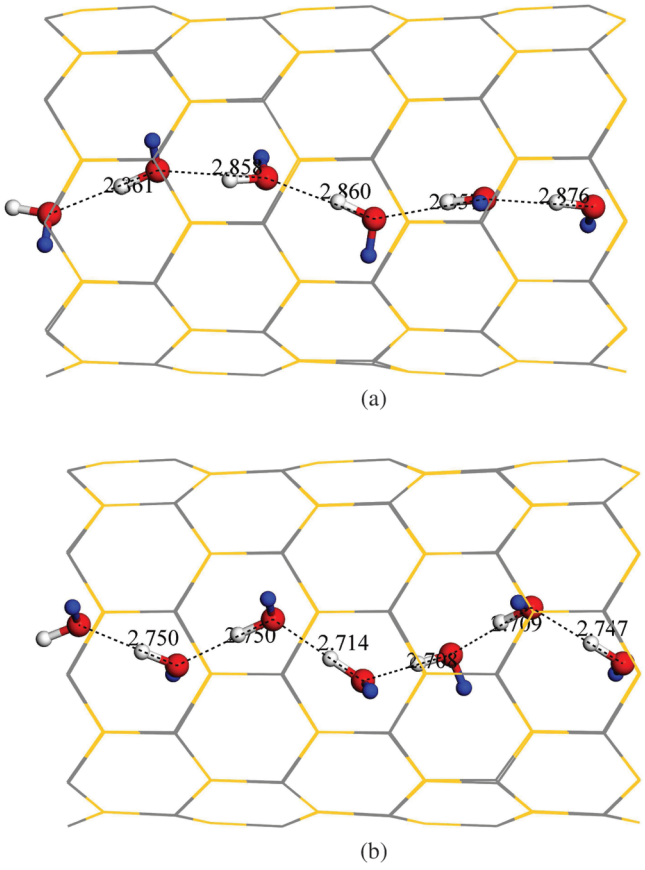

Figure 8. Water chain structure confined in SiCNT(9,0). (a) Six-water chain in SiCNT(9,0). (b) Seven-water chain in SiCNT(9,0).

water molecule number is also observed in other first-principles calculations of water confined in the SWCNT(6,6) system.[55] Since for the six-water system the R_{O-H} values and charges were found to be quite different between the hydrogen bonded and non-hydrogen-bonded hydrogen atoms, we proposed an "R-C" criteria that can be used to identify the two kinds of hydrogen atoms. Figure 6(b) shows an R-C plot for the $(H_2O)_7$ chain in the SiCNT(5,5) system. From this, it is clear that hydrogen-bonded H atoms are all located in one group with larger R_{O-H} and charge values compared to the non-hydrogen-bonded H atoms. The average R_{O-H} and charge values are 0.978 Å and 0.467e for the hydrogen-bonded H atoms and 0.963 Å and 0.157e for the non-hydrogen-bonded ones; this is comparable to those in the $(H_2O)_6$ chain. It is also easy to see from the figure that there are six hydrogen-bonded H atoms and eight non-hydrogen-bonded H atoms; these hydrogens have been colored white and blue in Figure 6(a). Clearly, the $(H_2O)_7$ system is also a chain fragment.

Single-Filed Infinite Water Chain in SiCNT(8,0), (9,0), and (10,0). We place six and seven water molecules in SiCNT(8,0), (9,0), and (10,0) to study water confined within zigzag SiCNT systems. In all cases, the water molecules formed infinite single-filed water chains as shown in Figure 7, Figure 8, and Figure 9.

It is noted that the O−H bond on the left end of the tube forms a H-bond with the right side water molecule in the neighboring supercell, giving rise to an infinite water chain. Each water molecule serves as both acceptor and donor in the chain to form two hydrogen bonds. The non-hydrogen-bonded O−H bond points toward the nanotube wall.

The supercell size, number density of water, structure parameters, and charges on the H atoms in the $(H_2O)_6$ and $(H_2O)_7$ chains for the three zigzag SiCNTs systems are listed in Table 2. Parameters for the water chain fragment confined in SiCNT(5,5) are also listed for comparison. All studied zigzag SiCNTs have similar supercell sizes of around 16.0 Å as listed in Table 2 but have different radius as listed in Table 1. The SiCNT(5,5) has a larger supercell size of around 18.54 Å. The number density of water is calculated using the 3D space enclosed within the SiCNT after subtracting the vdW radius of Si and C. In line with the increasing radius when going from the (8,0) to (9,0) and (10,0) systems, the number density of the $(H_2O)_6$ chain decreases from 0.028 to 0.013 $Å^{-3}$. Not surprisingly, the number density of the $(H_2O)_7$ chain is slightly larger than for the $(H_2O)_6$ chain in the same SiCNT. Although the number density of $(H_2O)_6$ or $(H_2O)_7$ in SiCNT(5,5) is comparable with those for SiCNT-(9,0), i.e., 0.018 or 0.021 $Å^{-3}$, the former can only form chain fragments. This suggests that the formation of an infinite water chain within the nanotube depends more on the length of the supercell rather than the available volume.

The R_{O-O} values for $(H_2O)_7$ are less than those of $(H_2O)_6$, but both keep increasing when going from SiCNT(8,0) to SiCNT(9,0) due to the larger available space. There is however no further increment in R_{O-O} in going from SiCNT(9,0) to SiCNT(10,0). This is because the space in both SiCNTs is large enough to contain an uncompressed one-dimensional water chain, albeit puckered. This puckering is evident from the increasing average distance between the oxygen atoms and the

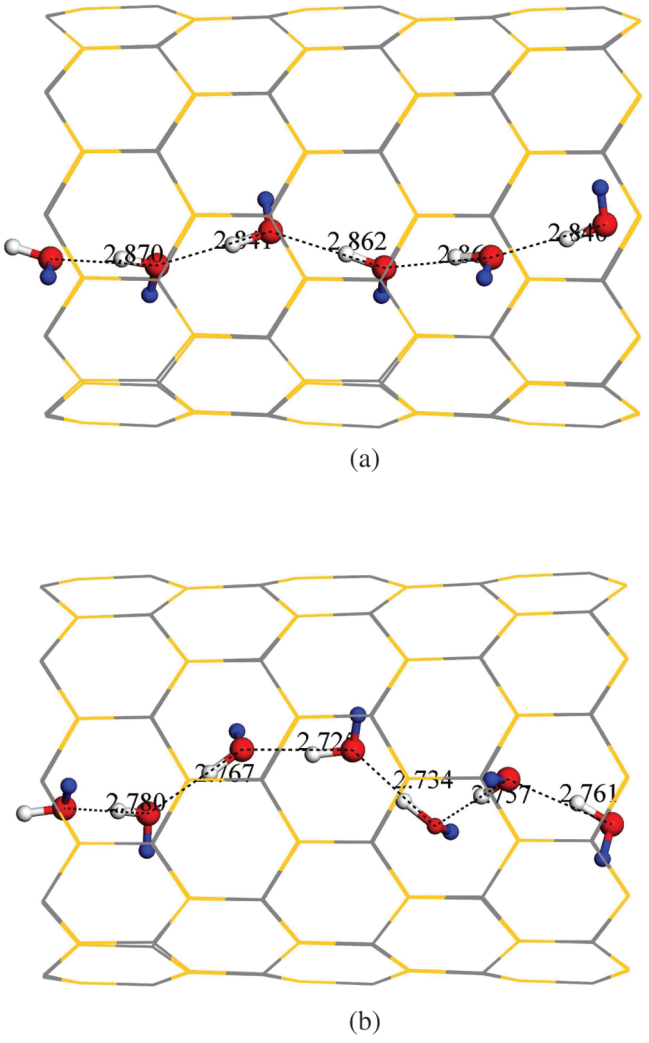

Figure 9. Water chain structure confined in zigzag SiCNT(10,0). (a) Six-water chain in SiCNT(10,0). (b) Seven-water chain in SiCNT(10,0).

center of the tube, Rad^{O}_{avg}, when going from the (8,0) to (9,0) and (10,0)SiCNT systems. Although the SiCNT(5,5) has a smaller radius than the SiCNT(9,0), the water chain fragment in the former tends to occupy a larger radius space than the latter as shown by its larger Rad^{O}_{avg}.

In all cases, each water molecule forms two hydrogen bonds ($N_b = 2$) no matter how many water molecules are involved. As for the armchair SiCNTs, the hydrogen-bonded H atoms have smaller R_{O-H} and larger charges than for those of the non-hydrogen-bonded H atoms. Between the $(H_2O)_6$ and $(H_2O)_7$ systems, the hydrogen-bonded R_{O-H} values increase slightly owing to the shorter R_{O-O} distance and the induced stretching of the O−H bond of the donor H atom. Between the different SiCNT systems, these values show much less variation. For the non-hydrogen-bonded H atoms, the R_{O-H} values are relatively insensitive to both the number of water molecules and to the SiCNT system.

In comparison to the slight variations in the R_{O-H} distance that occur as a function of hydrogen type, the number of water molecules, and the particular SiCNT system, the variation in the Mulliken charge on the hydrogen atoms is much larger. Here we see the charge on the hydrogen decreasing from the (8,0) to (9,0) and (10,0) SiCNT systems for the hydrogen-bonded hydrogen but increasing for the non-hydrogen-bonded hydrogen atom.

Table 2. Structure Parameters and Charges of Water Chain Confined in (8,0), (9,0), (10,0), and (5,5) SiCNTs

SiCNT	(8,0)	(9,0)	(10,0)	(5,5)
		Cell Size (in Å)		
$(H_2O)_6$	15.981	15.995	15.995	18.540
$(H_2O)_7$	15.989	15.989	16.010	18.546
		Number Density of Water (in $Å^{-3}$)		
$(H_2O)_6$	0.028	0.018	0.013	0.018
$(H_2O)_7$	0.032	0.021	0.015	0.021
		R_{O-O} (in Å)		
$(H_2O)_6$	2.775	2.862	2.856	2.771
$(H_2O)_7$	2.656	2.730	2.754	2.772
		Rad^{O}_{avg} (in Å)		
$(H_2O)_6$	0.445	0.651	0.945	0.751
$(H_2O)_7$	0.712	0.818	1.243	0.876
		Hydrogen-Bonded R_{O-H} (in Å)		
$(H_2O)_6$	0.974	0.973	0.973	0.983
$(H_2O)_7$	0.983	0.980	0.977	0.978
		Non-Hydrogen-Bonded R_{O-H} (in Å)		
$(H_2O)_6$	0.964	0.962	0.961	0.968
$(H_2O)_7$	0.963	0.961	0.960	0.963
		Charge of Hydrogen-Bonded H		
$(H_2O)_6$	0.501	0.478	0.462	0.467
$(H_2O)_7$	0.517	0.474	0.473	0.467
		Charge of Non-Hydrogen-Bonded H		
$(H_2O)_6$	0.124	0.180	0.205	0.167
$(H_2O)_7$	0.108	0.176	0.199	0.157

Structure of Multifiled Water Network in SiCNT(6,6). The number density of $(H_2O)_{17}$ within SiCNT(6,6) is 0.028 $Å^{-3}$, which is large enough to form a infinite water network. Figure 10-(a) and (b) shows an equilibrium system with 17 water molecules confined in SiCNT(6,6).

A water molecule forms 2−4 hydrogen bonds in the $(H_2O)_{17}$ network. Specifically, for the system shown there are three water molecules forming two hydrogen bonds ($N_2 = 3$), nine water molecules forming three hydrogen bonds ($N_3 = 9$), and five water molecules forming four hydrogen bonds ($N_4 = 5$). The average hydrogen bonds per water molecule, N_b, is 3.1. Both the value of N_b and the position of the maximum in the hydrogen bond distribution (at N_3) are lower than for bulk water, where N_b is 3.7 and most water molecules (58.2%) form four hydrogen bonds.[59] Interestingly, almost the same N_b value (around 3.0) and the same maximum in the H-bond distribution at N_3 were observed in simulations of water in a variety of SWCNT systems and rigid cylinders.[60] In that work, the authors conclude that the main variation in N_b is due to confinement effects rather than the particular type of interaction between the water and substrate (hydrophilic or hydrophobic). As the same distribution of hydrogen bonds and N_b value was obtained in this work and given that the tubes have comparable diameters, we contend that this conclusion probably also applies to SiCNT systems.

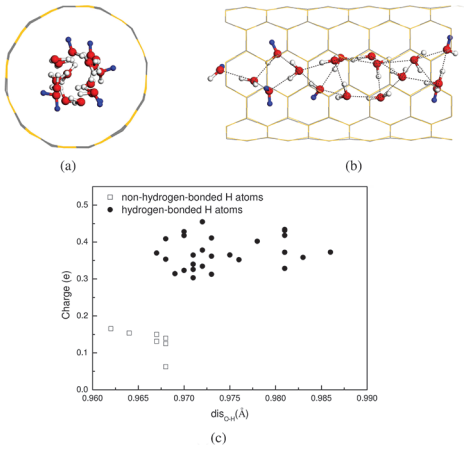

Figure 10. Structure and $R-C$ plot of the $(H_2O)_{17}$ network within SiCNT(6,6). (a) Radial view of the $(H_2O)_{17}$ network within SiCNT-(6,6). (b) Axial view of the $(H_2O)_{17}$ network within SiCNT(6,6). (c) $R-C$ plot for the 17-water network within SiCNT(6,6).

Table 3. Coupling Energy E_C, Binding Energy E_B, and H-Bond Strength E_{H-bond} from Both B3LYP and ωB97XD Functionals with and Without BSSE Corrections (in eV)

	B3LYP		ωB97XD			
systems	E_C	E_C^{BSSE}	E_C	E_C^{BSSE}	E_B^{BSSE}	E_{H-bond}^{BSSE}
Single-Filed Water Chain Fragments						
(5,5)+$(H_2O)_6$	−0.098	−0.015	−0.168	−0.078	−0.305	−0.227
(5,5)+$(H_2O)_7$	−0.066	0.009	−0.164	−0.068	−0.388	−0.320
Single-Filed Infinite Water Chain						
(8,0)+$(H_2O)_6$	−0.076	0.046	−0.265	−0.014	−0.331	−0.317
(8,0)+$(H_2O)_7$	−0.056	0.068	−0.151	−0.022	−0.320	−0.298
(9,0)+$(H_2O)_6$	−0.078	−0.001	−0.136	−0.054	−0.357	−0.303
(9,0)+$(H_2O)_7$	−0.077	0.004	−0.140	−0.054	−0.364	−0.310
(10,0)+$(H_2O)_6$	−0.058	−0.006	−0.101	−0.041	−0.343	−0.302
(10,0)+$(H_2O)_7$	−0.057	−0.002	−0.103	−0.039	−0.358	−0.319
Water Network						
(6,6)+$(H_2O)_{17}$	−0.067	−0.003	−0.116	−0.047	−0.403	−0.356

It is noted that the H atoms in water molecules at both ends of the supercell form hydrogen bonds with connecting water molecules in the neighboring supercell. Thus, the 17 water molecules in SiCNT(6,6) form an infinite multifiled network. The average R_{O-O} distance is 2.80 Å, which is larger than that for the single-filed water chain fragment in the SiCNT(5,5) system owing to the larger diameter of the nanotube and a weaker confinement effect.

The $R-C$ plot of the $(H_2O)_{17}$ network is given in Figure 10(c). R_{O-H} values are overlapped between the non-hydrogen-bonded and hydrogen-bonded H atoms owing to the complex hydrogen bond distribution. This makes it hard to identify the two kinds of H atoms according to structural information alone. Fortunately, the charges on the H atoms are much more sensitive to hydrogen bonding and combined with the R_{O-H} distance enable the hydrogens atoms to be classified into two groups as shown by the $R-C$ plot in Figure 10c. This shows that there are 7 non-hydrogen-bonded and 27 hydrogen-bonded H atoms.

Recent X-ray reflectivity measurements of the interface between water and the smooth hydrophobic monolayer conclusively show a water depletion layer with a substantially lower density than the bulk water density with a thickness of one water molecule.[61] In this work, all seven non-hydrogen-bonded O−H bonds point toward the nanotube wall as shown in Figure 10(a). Such dangling or "free" O−H bonds tend to reduce the number of hydrogen bonds in the water depletion region which can contribute to large flow rates in SWCNTs.[62] The similarity of the water structure in the depletion region between SiCNT and SWCNT may arise from the fact that water flow through both nanotubes is controlled by the confinement effect, and both nanotubes have a smooth surface.

Comparison of Binding Energies and Charge Transfer Across All Water Confined SiCNT Systems. Table 3 summarizes the coupling energy E_C and binding energy E_B per water molecule as defined in eq 1 and eq 3, respectively, and as obtained from both B3LYP and ωB97XD functionals. The superscript "BSSE" represents the term with basis set superposition error corrections.

The BSSE corrections reduce E_C to the extent that in several cases E_C^{BSSE} values are positive for the B3LYP functional. This is not the case when using the dispersion corrected ωB97XD functional, where all results remain negative after BSSE correction.

Although the BSSE correction decreases the values of E_C, the fact that the values of E_C^{BSSE} remain negative in all ωB97XD cases suggests that dispersion makes a significant contribution to the interaction between the water chain and the nanotube wall and cannot be neglected in such kinds of weakly bound systems. This need to account for dispersion has been clearly interpreted by performing both B3LYP and ωB97XD calculations in the present work and has also been shown for water-confined SWCNT systems.[63] Therefore, we will focus on the results from the ωB97XD calculations in the rest of this paper. It is worth noting that the dispersion effect could not only enhance E_C as listed in Table 3 but also enhance the hydrogen bondings as shown in Figure 1. As a result, the B3LYP and ωB97XD functionals obtained similar water structures confined within the SiCNT since they depend on the relative values of E_C and hydrogen bonding energy.

The very small E_C^{BSSE} values reflect the relatively weak interaction between the water molecules and the outer nanotube and suggest that the water molecules can flow through the nanotube almost "frictionless" with very high flow velocities. As the BSSE correction itself is sensitive to structural variations and is of a comparable size to the coupling energy, a slight structural variation between the water chain and the SiCNT can alter the coupling energy significantly. A notable trend is that the E_C^{BSSE} values in SiCNT(5,5) are stronger than for all studied zigzag SiCNTs, i.e., (8,0), (9,0), and (10,0). The stronger E_C^{BSSE} values tend to prevent the water molecules from flipping within the SiCNT. As a result, the six or seven water molecules within SiCNT(5,5) form water segments rather than the infinite water chains observed in zigzag SiCNTs despite the fact that both have very similar linear densities of water.

The BSSE corrected binding energies, E_B^{BSSE}, locate within 0.3−0.4 eV which are much larger than E_C^{BSSE} (less than 0.1 eV) for all studied systems as listed in Table 3. Both terms are comparable with those obtained in other first-principles studies of SWCNTs.[55,63] For example, the E_B and E_C of $(H_2O)_5$ within SWCNT(6,6) are 0.347 and 0.100 eV, respectively, obtained

Table 4. Average Charge Variation Per Atom upon the Water Chain Confined in SiCNTs for C, Si, O, and H Atoms Together with the Charge Transfer Per Water Molecule between the Water Chain and the SiCNT Wall, T

	C	Si	O	H	T
Single-Filed Water Chain Fragments					
(5,5)+$(H_2O)_6$	−0.012	0.022	−0.005	−0.047	−0.098
(5,5)+$(H_2O)_7$	−0.013	0.026	−0.011	−0.050	−0.112
Single-Filed Infinite Water Chain					
(8,0)+$(H_2O)_6$	−0.016	0.033	−0.033	−0.052	−0.137
(8,0)+$(H_2O)_7$	−0.017	0.037	−0.026	−0.057	−0.139
(9,0)+$(H_2O)_6$	−0.011	0.020	−0.020	−0.029	−0.078
(9,0)+$(H_2O)_7$	−0.014	0.024	−0.018	−0.030	−0.078
(10,0)+$(H_2O)_6$	−0.007	0.012	−0.012	−0.023	−0.057
(10,0)+$(H_2O)_7$	−0.009	0.016	−0.009	−0.024	−0.058
Water Network					
(6,6)+$(H_2O)_{17}$	−0.017	0.034	−0.009	−0.034	−0.076

from the GGA-PW91 calculations.[55] The E_C of an infinite water dimer chain within the SWCNT(6,6) are 0.159 eV by using GGA-PBE calculations.[63]

The hydrogen-bond strengths per water molecule, E^{BSSE}_{H-bond}, calculated as the difference between E^{BSSE}_C and E^{BSSE}_B are also listed in Table 3. For the water chain fragments confined in SiCNT(5,5), E^{BSSE}_{H-bond} gets stronger in going from $(H_2O)_6$ to $(H_2O)_7$, i.e., from −0.227 to −0.320 eV. This is due to a larger average number of hydrogen bonds per water molecule (N_b) that approaches the value obtained for an infinite water molecule chain confined in the zigzag SiCNTs. A similar dependence of the coupling energy on the number of water molecules is also observed in another first-principles study of SWCNTs.[55] For a single-filed infinite water chain within zigzag SiCNTs, values of E^{BSSE}_{H-bond} are almost independent of the number of water molecules owing to their fixed N_b value of 2. For the multifiled water network, i.e., $(H_2O)_{17}$ in SiCNT(6,6), N_b has a value of 3.1 which gives rise to a stronger E^{BSSE}_{H-bond} compared to any of the infinite single-filed water chains.

In Table 4, we present the variation of the average charge for each type of atom that occurs when placing the water chain into the SiCNTs together with the charge transfer that happens between the water chain and the SiCNT wall.

For all studied systems, the confinement of water gives rise to an increase in the ionic characteristic of the Si−C bonds, with C and Si becoming more negative and positive, respectively. This will give rise to a dipole−dipole interaction between the SiCNT and the molecules in the water chain. In addition, a slight charge transfer from SiCNT to the confined water molecules is observed in all cases, resulting in more negative charge on both the O and H atoms. Such charge transfer occurs locally from each water molecule to its nearest-neighbor Si−C pairs. With increasing diameter of the SiCNTs, the charge transfer becomes weaker. This is evident from the results for the infinite single-file water chain in the zigzag SiCNTs. However, there is no variation between cases with a different number of water molecules per supercell. Such charge transfer gives rise to extra bonding between the water chain and the SiCNTs in addition to those resulting from the vdW interactions.

The water transport process through a nanotube is composed of two consecutive steps: (a) entering the nanotube from the bulk and (b) flowing through the nanotube. Use of PBC models means that the focus of this paper has been on step (b). Although the SiC surface is hydrophilic, water molecules in SiCNT have structures and properties very similar to those of hydrophobic SWCNT systems, notably weak interactions between the water chain and nanotube wall, hydrogen bonding strength, and number distribution, consistent dependence of coupling energy and binding energy on the number of water molecules, etc. This implies that the behavior of water molecules encapsuled in SiCNTs is mainly affected by confinement effects rather than chemical effects, thus they are independent of the hydrophobicity of the nanotube. As hydrogen bonding governs the diffusion of water inside a nanotube, it is expected that water diffusion will be similar for both SiCNT and SWCNT.

Step (a) of water transport through a nanotube is controlled mainly by the pore-entrance effect, in which water molecules break hydrogen bonds between themselves to enable them to enter the nanotube. This is driven by the concentration gradient and thermal fluctuations. The pore-entrance effect is especially important for the transport of single-file water chains through narrow nanotubes as the energy barrier of water entering the pore increases with decreasing diameter of the nanotube. In addition, it is reported that the energy expense of breaking the network of hydrogen bonds in the bulk can be greatly compensated by attractive interactions between the fluid molecules and the hydrophilic entrance.[34] Considering the hydrophilic characteristic of the SiC surface, SiCNTs may be a promising artificial biological channel.

CONCLUSIONS

Using two hybrid DFT functionals, we have studied the structures and properties of water molecules confined in both armchair and zigzag SiCNTs. For all studied systems, ordered single-file water chains or multifiled water networks are formed. $R-C$ criteria are proposed to distinguish the hydrogen-bonded and non-hydrogen-bonded H atoms. According to this criteria, the former have longer O−H distance and larger charges than the latter. Including dispersion effects was found to be necessary to evaluate correctly the weak interaction between water and SiCNTs. We also found evidence for slight charge transfer from water to the SiCNT. For water within the SiCNT, the H-bond strength relates closely to the average H-bond number and increases from a single-filed water chain segment, to an infinite water chain, to a multifiled water network. Water molecules within the SiCNT have structures and properties similar to those encapsulated in hydrophobic SWCNTs since both are controlled by confinement effects. This makes SiCNT systems good potential candidates for artificial biological ion channels.

AUTHOR INFORMATION

Corresponding Author

*E-mail: ruiy@uow.edu.au.

Present Addresses

[§]University of Wollongong,Wollongong, NSW 2522 Australia.

■ ACKNOWLEDGMENT

This work is funded by Australian Research Council Linkage Grant LP0774896 and the National Health & Medical Research Council. Provision of computer time from the NCI National Facility is gratefully acknowledged.

■ REFERENCES

(1) Kalra, A.; Garde, S.; Hummer, G. *Proc. Natl. Acad. Sci. U.S.A.* **2003**, *100*, 10175.
(2) Weik, M.; Lehnert, U.; Zaccai, G. *Biophys. J.* **2005**, *89*, 3639.
(3) Murata, K.; Mitsuoka, K.; Hirai, T.; Walz, T.; Agre, P.; Haymann, J. B.; Engel, A.; Fujiyoshi, Y. *Nature* **2000**, *407*, 599.
(4) Srivastava, A.; Srivastava, O. N.; Talapatra, S.; Vajai, R.; Ajayan, P. M. *Nat. Mater.* **2000**, *3*, 610.
(5) Wang, Z.; Medforth, C. J.; Shelnutt, J. A. *J. Am. Chem. Soc.* **2004**, *126*, 16720.
(6) Gogotsi, Y.; Libera, J. A.; Yazicioglu, A. G.; Megaridis, C. M. *Appl. Phys. Lett.* **2001**, *79*, 1021.
(7) Naguib, N.; Ye, H.; Gogotsi, Y.; Yazicioglu, A. G.; Megaridis, C. M.; Yoshimura, M. *Nano Lett.* **2004**, *4*, 2237.
(8) Kolesnikov, A. I.; J. M. Zanotti, J. M. C. K. L.; Thiyagarajan, P.; Moravsky, A. P.; Loutfy, R. O.; Burnham, C. J. *Phys. Rev. Lett.* **2004**, *93*, 035503.
(9) Hummer, G.; Rasaiah, J. C.; Noworyta, J. P. *Nature* **2001**, *414*, 188.
(10) Maibaum, L.; Chandler, D. *J. Phys. Chem. B* **2003**, *107*, 11891189.
(11) Beckstein, O.; Sansom, M. S. P. *Proc. Natl. Acad. Sci. U.S.A.* **2003**, *100*, 7063.
(12) Holt, J. K.; Park, H. P.; Waang, Y.; Stadermann, M.; Artyukhin, A. B.; Grigopoupulos, C. P.; Noy, A.; Bakajin, O. *Science* **2006**, *312*, 1034.
(13) Majumder, M.; Chopra, N.; Andrews, R.; Hinds, B. J. *Nature* **2005**, *438*, 44.
(14) Mashl, R. J.; Joseph, S.; Aluru, N. R.; Jakobsson, E. *Nano Lett.* **2003**, *3*, 589.
(15) Koga, K.; Gao, G. T.; Tanaka, H.; Zeng, X. C. *Nature* **2001**, *412*, 802.
(16) Chandler, D. *Nature* **2005**, *437*, 640.
(17) Fang, H. P.; Wan, R. Z.; Gong, X. J.; Lu, H. J.; Li, S. Y. *J. Phys. D: Appl. Phys.* **2008**, *41*, 103002.
(18) Won, C. Y.; Aluru, N. R. *J. Am. Chem. Soc.* **2007**, *129*, 2748–2749.
(19) Won, C. Y.; Aluru, N. R. *J. Phys. Chem. C* **2008**, *112*, 1812–1818.
(20) Yuan, Q. Z.; Zhao, Y. P. *J. Am. Chem. Soc.* **2009**, *131*, 6374–6376.
(21) Pham-Huu, C.; Keller, N.; Ehret, G.; J.Ledouxi, M. *J. Catal.* **2001**, *200*, 400.
(22) Sun, X. H.; Li, C. P.; Wong, W. K.; Wong, N. B.; Lee, C. S.; T. Lee, S.; Teo, B. T. *J. Am. Chem. Soc.* **2002**, *124*, 14464.
(23) Keller, N.; Pham-Huu, C.; Ehret, G.; Keller, V.; Ledous, M. J. *Carbon* **2003**, *41*, 2131.
(24) Borowiak-Palen, E.; Ruemmeli, M. H.; Gemming, T.; Knupfer, M.; Biedermann, K.; Leonhardt, A.; Pihler, T.; Kalenczuk, R. J. *J. Appl. Phys.* **2005**, *97*, 056102.
(25) Taguchi, T.; Igawa, N.; Yamamoto, H.; Shamoto, S.; Jitsukawa, S. *Phys. E (Amsterdam, Neth.)* **2005**, *28*, 431.
(26) Hu, J. Q.; Bando, Y.; Zhan, J. H.; Goberg, D. *Appl. Phys. Lett.* **2004**, *85*, 2923.
(27) Nhut, J. M.; Vieira, R.; Pesant, L.; Tessonnier, J.-P.; Keller, N.; Ehet, G.; Pham-Huu, C.; Ledoux, M. J. *Catal. Today* **2002**, *79*, 11.
(28) Taguchi, T.; Igawa, N.; Yamamoto, H.; Jitsukawa, S. *J. Am. Ceram. Soc.* **2005**, *88*, 459.
(29) Huczko, A.; Bystrzejewski, M.; Lange, H.; Fabianowska, A.; Cudzilo, S; Panas, A.; Szala, M. *J. Phys. Chem. B* **2005**, *109*, 16244.
(30) Zhang, Y. F.; Huang, H. C. *Comput. Mater. Sci.* **2008**, *43*, 664–669.
(31) Mpournpakis, G.; Froudakis, G. E.; lithoxoos, G. P.; Samios, J. *Nano Lett.* **2006**, *6*, 1581.
(32) Zhao, M. W.; Xia, Y. Y.; Li, F.; Zhang, R. Q.; Lee, S. T. *Phys. Rev. B* **2005**, *71*, 085312.
(33) Cicero, G.; Galli., G. *J. Phys. Chem. B* **2004**, *108*, 16518.
(34) Zheng, J.; Lennon, E.; Y. H. Sheng, H. K. T.; Jiang, S. *J. Chem. Phys.* **2005**, *122*, 214702.
(35) Alam, K. M.; Ray, A. K. *Nanotechnology* **2007**, *18*, 495706.
(36) Alam, K. M.; Ray, A. K. *Phys. Rev. B* **2008**, *77*, 035436.
(37) CPMD, Copyright IBM Corp 1990−2008 and Copyright MPI für Festkörperforschung Stuttgart 1997−2001.
(38) Frisch, M. J. et al. *Gaussian 09*, revision A.1; Gaussian Inc.: Wallingford CT, 2009.
(39) Tsuzuki, S.; Lüthi, H. P. *J. Chem. Phys.* **2001**, *114*, 3949–3957.
(40) Chai, J. D.; Head-Gordon, M. *Phys. Chem. Chem. Phys.* **2008**, *10*, 6615–6620.
(41) Klopper, W.; van Duijneveldt-van de Rijdt, J. G. C. M.; van Duijneveldt, F. B. *Phys. Chem. Chem. Phys.* **2000**, *10*, 2227–2234.
(42) Anderson, J. A.; Tschumper, G. S. *J. Phys. Chem. A* **2006**, *110*, 7268–7271.
(43) Tschumper, G. S.; Leininger, M. L.; Hoffman, B. C.; Valeev, E. F.; Schaefer, H. F.; Quack, M. *J. Chem. Phys.* **2002**, *116*, 690–701.
(44) Gao, G. H.; Park, S. H.; Kang, H. S. *Chem. Phys.* **2009**, *355*, 50–54.
(45) Gali, A. *Phys. Rev. B* **2006**, *73*, 245415.
(46) Moradian, R.; Behzad, S.; Chegel, R. *Phys. B* **2008**, *403*, 3623–3626.
(47) Moon, W. H.; Ham, J. K.; Hwang, H. J. *Nanotechnology* **2003**, *3*, 158.
(48) Menon, M.; Richter, E.; Mavrandonakis, A.; Froudakis, G.; Andriotis, A. *Phys. Rev. B* **2004**, *69*, 115322.
(49) Saito, R.; Fujiata, M.; G, G. D.; Dresselhaus, M. S. *Appl. Phys. Lett.* **1992**, *60*, 2204.
(50) Mavrandonakis, A.; G. E. Froudakis, M. S.; Muhlhauser, M. *Nano Lett.* **2003**, *3*, 1481.
(51) Rubio, A.; Corkill, J. L.; Cohen, M. L. *Phys. Rev. B* **1994**, *49*, 5081.
(52) Zhao, M. W.; Xia, Y. Y.; Zhang, D. J.; Mei, L. M. *Phys. Rev. B* **2003**, *68*, 235415.
(53) Lee, S. M.; Lee, Y. H.; Hwang, Y. G.; Elsner, J.; Porezag, D.; Frauenheim, Th. *Phys. Rev. B* **1999**, *60*, 7788.
(54) Huang, S. P.; Wu, D. S.; Hu, J. M.; Zhang, H.; Xie, Z.; Hu, H.; Cheng, W. D. *Opt. Express* **2007**, *15*, 10947.
(55) Wang, L.; Zhao, J. J.; Li, F. Y.; Fang, H. P.; Lu, J. P. *J. Phys. Chem. C* **2009**, *113*, 5368–5375.
(56) Xu, H.; Berne, B. J. *J. Phys.: Condens. Matter* **2001**, *105*, 11929.
(57) Hanasaki, I.; Nakamura, A.; Yonebayashi, T.; Kawano, S. *J. Phys.: Condens. Matter* **2008**, *20*, 015213.
(58) Mann, D. J.; halls, M. D. *Phys. Rev. Lett.* **2003**, *90*, 195503.
(59) Mart, J. *J. Chem. Phys.* **1999**, *110*, 6876.
(60) Gordillo, M. C.; Mart, J. *J. Chem. Phys.* **2000**, *329*, 341.
(61) Poynor, A.; Hong, L.; Robinson, I. K.; Granick, S.; Zhang, Z.; Fenter, P. A. *Phys. Rev. Lett.* **2006**, *97*, 266101.
(62) Joseph, S.; Aluru, N. R. *Nano Lett.* **2008**, *8*, 452.
(63) K.Agrawal, B.; Singh, V.; Pathak, A.; Srivastava, R. *Phys. Rev. B* **2007**, *75*, 195421.